 CMES, vol.109-110, no.1, pp.1-13, 2015

First-principles Calculation of Interfacial Adhesion Strength and Electromigration for the Micro-bump Interconnect of 3D Chip Stacking Packaging

W.H. Chen[1], H.C. Cheng[2,3] and C.F. Yu[1,3]

Abstract: This study aims at exploring the interfacial adhesion strength between solder bump and four typical under bump metallurgies (UBMs), i.e., Cu/Ni, Cu/TiW, Cu/Ni/Cr and /Cu/V/Cr, at atomistic scale. The average bond length and interfacial adhesion stress of the Sn-3.5Ag/Cu/Ni, Sn-3.5Ag/Cu/TiW, Sn-3.5Ag/Cu/Ni/Cr and Sn-3.5Ag/Cu/V/Cr micro-bump interconnects are calculated through the first-principles density functional theory (DFT) calculation to estimate the interfacial adhesion strength between the solder bump and UBMs. In addition, by investigating the electric field effect on the average bond length and adhesive stress, the combination of solder bump and UBM with better interfacial adhesion strength and electromigration resistance ability can be determined. The results show that the interfacial adhesion strength between solder bump and wetting layer is much weaker than those of other interfaces, implying that the interfacial failure, induced by the electromigration, is likely to occur at the interface between solder bump and wetting layer. It is also found that the Sn-3.5Ag/Cu/Ni micro-bump interconnect would possess much stronger interfacial adhesion strength at the interface between solder bump and wetting layer than the other micro-bump interconnects. In addition, in comparison with the TiW and V metals, the Ni metal as the diffusion barrier layer can yield much stronger interfacial adhesion strength with wetting layer. Finally, as the adhesion layer is made of Cr metal, the Ni metal, acting as diffusion barrier layer, would hold much stronger interfacial adhesion strength than that of V metal.

Keywords: Interfacial adhesion strength, Under bump metallurgy, First-principles density functional theory calculation, Solder bump.

[1] Department of Power Mechanical Engineering, National Tsing Hua University, Hsinchu, Taiwan, ROC.

[2] Department of Aerospace and Systems Engineering Feng Chia University, Taichung, Taiwan, ROC.

[3] Corresponding author.

1 Introduction

Nowadays, because of the ever-increasing demands for mobile devices with great functional diversification, heterogeneity, miniaturization and high performance, integration of multi-media functions using three-dimensional (3D) integrated circuit (IC) packaging technology has become increasingly essential and crucial [Chen, Yu, Cheng, Tsai, and Lu (2013); Cheng, Cheng, Lu, Juang, and Chen (2014); Hu, Cheng, Huang, Chen, Wu, and Lo (2015)]. To achieve the challenges, aside from the revolution of IC circuit design, great engineering efforts are presently being placed on the development of high-reliability, high-performance 3D chip stacking packaging with micro-bump interconnect and through silicon via (TSV) technology [Cheng, Tsai, Chen, and Fang (2010); Cheng, Hsieh, and Chen (2011); Cheng, Hsieh, and Chen (2014)]. Compared with other flip chip technology, there are many implied advantageous characterizations in the packaging technology, such as increased function density, reduced package profile and interconnect length, and enhanced electrical performance. Figure 1 shows schematic configuration of the micro-bump interconnect, which consists of solder bump and under bump metallurgy (UBM). In specific, the solder bump is commonly made up of Sn-3.5Ag alloy, and the UMB generally consists of wetting layer, diffusion barrier layer and adhesion layer [Patterson Elenius, and Leal (1997)].

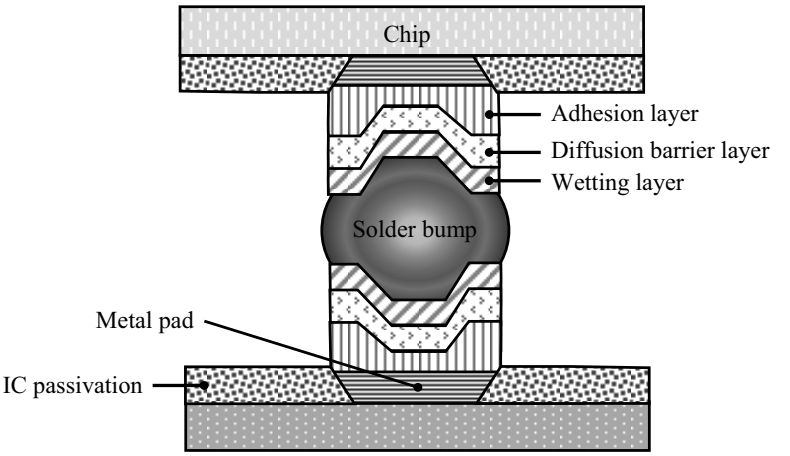

Figure 1: Schematic configuration of the micro-bump interconnect

Signal between the chip and micro-bump interconnect is connected by way of the metal pad. The wetting layer, normally made up of Cu metal, is used to increase the wettability of the solder bump. To prevent the chemical diffusion between metal pad and solder bump, the diffusion barrier layer is adopted, which is made up of Ni,

V and TiW metals. Moreover, the Cr metal is always applied as adhesion layer to enhance the interfacial adhesion strength between metal pad and passivation layer. In recent, because of miniaturization of the characteristic dimension of IC, the scale of standard fabrication process of wafer level packaging can reduce down to 22 nm and even more Moore (i.e., 11 nm) and beyond CMOS. At this miniaturization trend, the dimension of 3D chip stacking packaging is bound to submicron. Thus, the dimension of the solder bump and UBM is likely to down to nanoscale. Notably, at such scale, the micro-bump interconnect of the 3D chip stacking packaging usually endures the high local temperature/mechanical stresses during shipping, handling, transportation, and lifetime usage [Fan and Yuen (2010)]. Consequently, if the interfacial adhesion strength between solder bump and UBM is not strong enough, several damage phenomena, such as delamination [Wu, Paik, and Bhandarkar (1995)], crack [Yang, Lai, Jian, and Chen (2007)] and even fracture [Cheng, Cheng, Lu, Juang, and Chen (2013)], can be observed at the interfaces either between solder bump and wetting layer, wetting layer and diffusion barrier layer, or diffusion barrier layer and adhesion layer, as a result potentially leading to open circuit failure for electronic component.

Besides, in addition to the interfacial failure induced by the temperature/mechanical stresses, the well-known electromigration phenomenon [Cheng, Yu, and Chen (2014a)] is also found at the micro-bump interconnect. The electromigration is a mass transport phenomenon, in which, metal atoms migrate along the direction of electron flux [Iwasaki and Miura (2003); Gerstle, Silling, Read, Tewary, and Lehoucq (2008)]. The directional diffusion would lead to the formation of hillocks at the anode side and voids at the cathode side of the solder bump. This phenomenon would induce the signal delay, distortion or even short-circuit failure for electronic component under long-firing operation, thereby leading to a decrease of the electronic component reliability. In addition, the current density of the micro-bump interconnect would substantially increase as dimension of the solder bump becomes smaller, thus resulting in a significant current crowding effect [Cheng, Yu, and Chen (2014a)]. The current effect is a nonhomogeneous distribution of current density, which can remarkably enhance the electromigration phenomenon of the solder bump.

To sum up, the fatigue life of the micro-bump interconnect for the 3D chip stacking packaging technology is remarkably influenced by the interfacial adhesion strength between solder bump and UBM. Therefore, the goal of the study is to calculate the average bond length and interfacial adhesion stress through the first-principles density functional theory (DFT) calculation [Hohenberg and Kohn (1964); Perdew, Burke, and Ernzerhof (1996); Branden and Cristian (2013); Cheng, Yu, and Chen (2014b)] for evaluating the interaction between solder bump and wetting layer, wet-

ting layer and diffusion barrier layer, and diffusion barrier layer and adhesion layer. In addition, by imposing the external electric field, the electromigration effect on the average bond length and interfacial adhesion stress also can be explored. Finally, the combination of solder bump and UBM with better interfacial adhesion strength can be determined.

2 Computational details

Four types of micro-bump interconnects, i.e., Sn-3.5Ag/Cu/Ni, Sn-3.5Ag/Cu/TiW, Sn-3.5Ag/Cu/Ni/Cr and Sn-3.5Ag/Cu/V/Cr, are investigated in the study, and the corresponding atomic models are exhibited in Fig. 2. It is found that the wetting layer, diffusion barrier layer and adhesion layer are composed of two atomic layers. To achieve the atomic model of Sn-3.5Ag alloy, the substitutional solid solution rule is used. The rule has been widely utilized for constructing the uniform composition distribution in alloy system [Cheng, Yu, and Chen (2014b)]. By the rule, the Sn and Ag atoms can thus uniformly distribute in the Sn-3.5Ag alloy system. For enhancement of the computational efficiency, the periodic boundary condition is further imposed to the atomic models along x and y axes. Two magnitude of external electric field, i.e., 0.05 and 0.1 V/Å, are applied to investigate the electromigration effect on the interfacial adhesion strength, and the external electric field direction is [0 0 1], as demonstrated in Fig. 3.

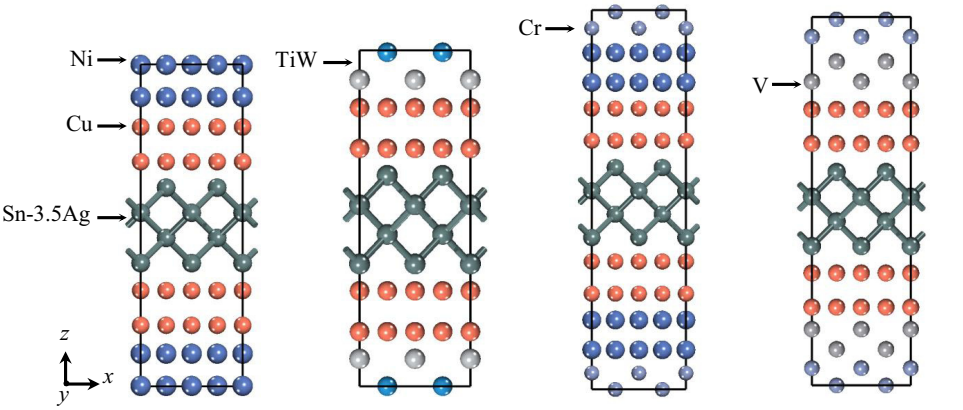

(a) Sn-3.5Ag/Cu/Ni (b)Sn-3.5Ag/Cu/TiW (c) Sn-3.5Ag/Cu/Ni/Cr (d) Sn-3.5Ag/Cu/V/Cr

Figure 2: Atomic crystal structures of four types of micro-bump interconnects

In the study, all the calculations are carried out using the first-principles DFT calculation through Cambridge Serial Total Energy Package (CASTEP) code [Yu,

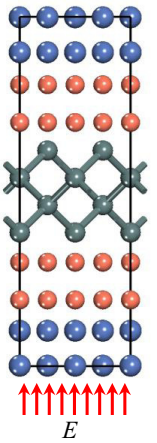

Figure 3: Direction of the applied external electric field

Cheng, and Chen (2015); Chen, Yu, Chiang, and Cheng (2015)]. The Vanderbilt's ultrasoft pseudopotential scheme [Vanderbilt (1990)] is further utilized to model the interactions of valence electrons with ion cores. The exchange-correlation potential is calculated within the generalized gradient approximation (GGA) using the Perdew-Burke-Ernzerhof (PBE) correlation functional [Perdew, Burke, and Ernzerhof (1996)], which depends on both the electron density and its gradient at each space point. The well-known Broyden-Fletcher-Goldfarb-Shanno (BFGS) variable-metric minimization algorithm [Head (1985)] is then utilized to seek the ground state or geometry optimization. It has been demonstrated that the technique is very efficient and robust to explore the optimal minimal energy crystalline structure. The plane wave basis set is truncated using a cutoff energy of 440 eV. To sample the Brillouin zone [Brillouin (1930)], the Monkhorst-Pack k-point mesh [Monkhorst and Pack (1976)] is employed. It is selected based on the convergence of the k-point mesh, where the change of total energy becomes less than 1 meV/atom. In the study, the selected k-point mesh is $3 \times 3 \times 1$. The convergence conditions considered in the geometry optimization include an energy tolerance of 2×10^5 eV/atom, maximum ionic Hellmann-Feynman force within 0.01 eV/Å, maximum stress within 0.02 GPa and maximum ionic displacement within 5×10^{-4} Å.

3 Result and discussion

The average bond lengths are first calculated to evaluate the electromigration resistance ability for the interfaces at solder bump and wetting layer, wetting layer

and diffusion barrier layer, and diffusion barrier layer and adhesion layer. The average bond length has been successfully utilized to estimate the electromigration resistance ability for layered structures [Cheng, Yu, and Chen (2014a)]. Table 1 shows the calculated average bond lengths for all interfaces at the electric field of 0.05 V/Å and 0.1 V/Å. It is now recognized that the average bond lengths for the interfaces at different locations are not identical, and schematic presentation of the average bond lengths in micro-bump interconnect is shown in Fig. 4. The results in Table 1 indicate that the value of average bond length between solder bump and wetting layer below the solder bump (i.e., ${}^{bottom}d^{ave}_{\text{Sn-3.5Ag/Cu}}$) is obviously larger than that between solder bump and wetting layer above the solder bump (i.e., ${}^{top}d^{ave}_{\text{Sn-3.5Ag/Cu}}$). It is attributed that the Sn atoms in solder bump are driven by the external electric field with the direction of [0 0 1]. Thus, it can be also found that the interfacial failure is likely to occur at the interface between solder bump and wetting layer below the solder bump.

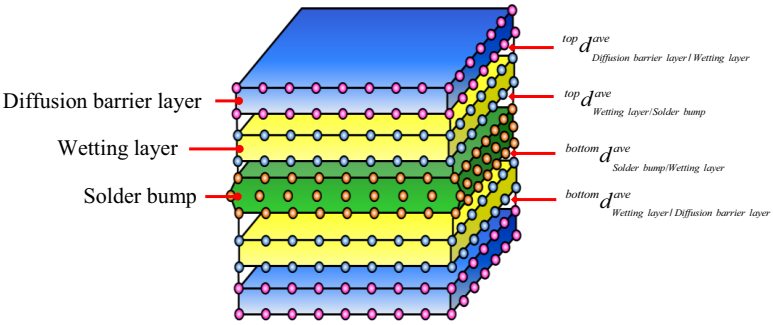

Figure 4: Schematic presentation of the average bond lengths in micro-bump

Table 1 also shows that ${}^{bottom}d^{ave}_{\text{Sn-3.5Ag/Cu}}$ and ${}^{top}d^{ave}_{\text{Sn-3.5Ag/Cu}}$ increases with the increase of electric field, implying that the interfacial adhesion strength between solder bump and copper layer reduces with the increasing electric field. At the electric field of 0.05 V/Å, it is observed that ${}^{top}d^{ave}_{\text{Sn-3.5Ag/Cu}}$ and ${}^{bottom}d^{ave}_{\text{Sn-3.5Ag/Cu}}$ for the micro-bump interconnect type of Sn-3.5Ag/Cu/Ni, Sn-3.5Ag/Cu/TiW, Sn-3.5Ag/Cu/Ni/Cr and Sn-3.5Ag/Cu/V/Cr are 1.91 Å and 2.54 Å, 2.60 Å and 2.82 Å, 2.12 Å and 2.71 Å, and 2.81 Å and 3.19 Å. The results reveal that the Sn-3.5Ag/Cu/Ni holds the strongest interfacial adhesion strength at the interface between solder bump and copper layer, followed by Sn-3.5Ag/Cu/Ni/Cr, Sn-3.5Ag/Cu/TiW and Sn-3.5Ag/Cu/V/Cr. Table 1 further shows that the average bond length between wetting layer and diffusion barrier layer for Sn-3.5Ag/Cu/Ni, Sn-3.5Ag/Cu/TiW, Sn-3.5Ag/Cu/Ni/Cr and Sn-3.5Ag/Cu/V/Cr (i.e., ${}^{top^I}d^{ave}_{\text{Cu/Ni}}$ and ${}^{bottom^I}d^{ave}_{\text{Cu/Ni}}$, ${}^{top}d^{ave}_{\text{Cu/TiW}}$ and ${}^{bottom}d^{ave}_{\text{Cu/TiW}}$, ${}^{top^{II}}d^{ave}_{\text{Cu/Ni}}$ and ${}^{bottom^{II}}d^{ave}_{\text{Cu/Ni}}$, and ${}^{top}d^{ave}_{\text{Cu/V}}$ and

Table 1: The average bond lengths of all interfaces as a function of electric field

Micro-bump type	Electric field (V/Å)	Average bond length (Å)	
Sn-3.5Ag/Cu/Ni	0.05	$^{top^{I}}d^{ave}_{\text{Cu/Ni}}$	1.27
		$^{top}d^{ave}_{\text{Sn-3.5Ag/Cu}}$	1.91
		$^{bottom}d^{ave}_{\text{Sn-3.5Ag/Cu}}$	2.54
		$^{bottom^{I}}d^{ave}_{\text{Cu/Ni}}$	1.30
	0.1	$^{top^{I}}d^{ave}_{\text{Cu/Ni}}$	1.32
		$^{top}d^{ave}_{\text{Sn-3.5Ag/Cu}}$	2.23
		$^{bottom}d^{ave}_{\text{Sn-3.5Ag/Cu}}$	2.82
		$^{bottom^{I}}d^{ave}_{\text{Cu/Ni}}$	1.37
Sn-3.5Ag/Cu/TiW	0.05	$^{top}d^{ave}_{\text{Cu/TiW}}$	2.50
		$^{top}d^{ave}_{\text{Sn-3.5Ag/Cu}}$	2.60
		$^{bottom}d^{ave}_{\text{Sn-3.5Ag/Cu}}$	2.82
		$^{bottom}d^{ave}_{\text{Cu/TiW}}$	2.56
	0.1	$^{top}d^{ave}_{\text{Cu/TiW}}$	2.95
		$^{top}d^{ave}_{\text{Sn-3.5Ag/Cu}}$	2.82
		$^{bottom}d^{ave}_{\text{Sn-3.5Ag/Cu}}$	3.16
		$^{bottom}d^{ave}_{\text{Cu/TiW}}$	3.02
Sn-3.5Ag/Cu/Ni/Cr	0.05	$^{top}d^{ave}_{\text{Ni/Cr}}$	2.21
		$^{top^{II}}d^{ave}_{\text{Cu/Ni}}$	1.75
		$^{top}d^{ave}_{\text{Sn-3.5Ag/Cu}}$	2.12
		$^{bottom}d^{ave}_{\text{Sn-3.5Ag/Cu}}$	2.71
		$^{bottom^{II}}d^{ave}_{\text{Cu/Ni}}$	1.78
		$^{bottom}d^{ave}_{\text{Ni/Cr}}$	2.26
	0.1	$^{top}d^{ave}_{\text{Cu/TiW}}$	2.44
		$^{top}d^{ave}_{\text{Sn-3.5Ag/Cu}}$	1.82
		$^{bottom}d^{ave}_{\text{Sn-3.5Ag/Cu}}$	2.56
		$^{bottom}d^{ave}_{\text{Cu/TiW}}$	2.88
		$^{top}d^{ave}_{\text{Cu/TiW}}$	1.86
		$^{top}d^{ave}_{\text{Sn-3.5Ag/Cu}}$	2.50
Sn-3.5Ag/Cu/V/Cr	0.05	$^{top}d^{ave}_{\text{V/Cr}}$	2.52
		$^{top}d^{ave}_{\text{Cu/V}}$	2.61
		$^{top}d^{ave}_{\text{Sn-3.5Ag/Cu}}$	2.81
		$^{bottom}d^{ave}_{\text{Sn-3.5Ag/Cu}}$	3.19
		$^{bottom}d^{ave}_{\text{Cu/V}}$	2.66
		$^{bottom}d^{ave}_{\text{V/Cr}}$	2.62
	0.1	$^{top}d^{ave}_{\text{V/Cr}}$	2.73
		$^{top}d^{ave}_{\text{Cu/V}}$	2.71
		$^{top}d^{ave}_{\text{Sn-3.5Ag/Cu}}$	3.05
		$^{bottom}d^{ave}_{\text{Sn-3.5Ag/Cu}}$	3.36
		$^{bottom}d^{ave}_{\text{Cu/V}}$	2.62
		$^{bottom}d^{ave}_{\text{V/Cr}}$	2.77

Table 2: The interfacial adhesion strengths of all interfaces as a function of electric field

	Electric field (V/Å)	Interfacial adhesion strength (GPa)	
Sn-3.5Ag/Cu/Ni	0.05	$^{top^{I}}\sigma^{ave}_{Cu/Ni}$	30.16
		$^{top}\sigma^{ave}_{Sn\text{-}3.5Ag/Cu}$	17.39
		$^{bottom}\sigma^{ave}_{Sn\text{-}3.5Ag/Cu}$	12.08
		$^{bottom^{I}}\sigma^{ave}_{Cu/Ni}$	29.54
	0.1	$^{top^{I}}\sigma^{ave}_{Cu/Ni}$	27.92
		$^{top}\sigma^{ave}_{Sn\text{-}3.5Ag/Cu}$	9.42
		$^{bottom}\sigma^{ave}_{Sn\text{-}3.5Ag/Cu}$	6.76
		$^{bottom^{I}}\sigma^{ave}_{Cu/Ni}$	27.30
Sn-3.5Ag/Cu/TiW	0.05	$^{top}\sigma^{ave}_{Cu/TiW}$	22.17
		$^{top}\sigma^{ave}_{Sn\text{-}3.5Ag/Cu}$	12.06
		$^{bottom}\sigma^{ave}_{Sn\text{-}3.5Ag/Cu}$	7.87
		$^{bottom}\sigma^{ave}_{Cu/TiW}$	21.58
	0.1	$^{top}\sigma^{ave}_{Cu/TiW}$	20.13
		$^{top}\sigma^{ave}_{Sn\text{-}3.5Ag/Cu}$	9.57
		$^{bottom}\sigma^{ave}_{Sn\text{-}3.5Ag/Cu}$	6.57
		$^{bottom}\sigma^{ave}_{Cu/TiW}$	19.53
Sn-3.5Ag/Cu/Ni/Cr	0.05	$^{top}\sigma^{ave}_{Ni/Cr}$	16.57
		$^{top^{II}}\sigma^{ave}_{Cu/Ni}$	26.03
		$^{top}\sigma^{ave}_{Sn\text{-}3.5Ag/Cu}$	14.13
		$^{bottom}\sigma^{ave}_{Sn\text{-}3.5Ag/Cu}$	9.50
		$^{bottom^{II}}\sigma^{ave}_{Cu/Ni}$	25.57
		$^{bottom}\sigma^{ave}_{Ni/Cr}$	16.15
	0.1	$^{top}\sigma^{ave}_{Ni/Cr}$	11.65
		$^{top^{II}}\sigma^{ave}_{Cu/Ni}$	23.72
		$^{top}\sigma^{ave}_{Sn\text{-}3.5Ag/Cu}$	8.01
		$^{bottom}\sigma^{ave}_{Sn\text{-}3.5Ag/Cu}$	6.42
		$^{bottom^{II}}\sigma^{ave}_{Cu/Ni}$	23.21
		$^{bottom}\sigma^{ave}_{Ni/Cr}$	11.24
Sn-3.5Ag/Cu/V/Cr	0.05	$^{top}\sigma^{ave}_{V/Cr}$	14.59
		$^{top}\sigma^{ave}_{Cu/V}$	18.32
		$^{top}\sigma^{ave}_{Sn\text{-}3.5Ag/Cu}$	9.80
		$^{bottom}\sigma^{ave}_{Sn\text{-}3.5Ag/Cu}$	6.79
		$^{bottom}\sigma^{ave}_{Cu/V}$	17.88
		$^{bottom}\sigma^{ave}_{V/Cr}$	13.85
	0.1	$^{top}\sigma^{ave}_{V/Cr}$	13.75
		$^{top}\sigma^{ave}_{Cu/V}$	16.50
		$^{top}\sigma^{ave}_{Sn\text{-}3.5Ag/Cu}$	8.52
		$^{bottom}\sigma^{ave}_{Sn\text{-}3.5Ag/Cu}$	5.82
		$^{bottom}\sigma^{ave}_{Cu/V}$	15.89
		$^{bottom}\sigma^{ave}_{V/Cr}$	13.20

${}^{bottom}d^{ave}_{Cu/V}$) are around 1.27 Å and 1.30 Å, 2.56 Å and 2.50 Å, 1.75 Å and 1.78 Å, and 2.61 Å and 2.66 Å. Clearly, the Ni metal, acting as diffusion barrier layer, would hold the largest interfacial adhesion strength with wetting layer, followed by TiW and V metals. In addition, it is found that as the adhesion layer is made of Cr metal, the Ni metal, acting as diffusion barrier layer, would hold much larger interfacial adhesion strength than that of V metal.

The Nielsen-Martin stress theorem [Nielsen and Martin (1987)] is also applied in the study to calculate the interfacial adhesion stress for Sn-3.5Ag/Cu/Ni, Sn-3.5Ag/Cu/TiW, Sn-3.5Ag/Cu/Ni/Cr and Sn-3.5Ag/Cu/V/Cr micro-bump interconnects. The formula of Nielsen-Martin stress theorem is shown in the following equation,

$$\sigma_{ij} = \frac{1}{V}\frac{\partial U}{\partial \varepsilon_{ij}}, \tag{1}$$

where σ_{ij} is the interfacial adhesion stress, V is the volume of the interface and ε_{ij} is tensile strain. The strain energy U of the interface is calculated by strain ε_{ij} resulting from changing the displacement of the atoms on the interface. By the U-ε_{ij} relation obtained from curve-fitting analysis, the first derivative of the strain energy with respect to the strain yields the interfacial adhesion stress according to Eq. (1). The largest interfacial adhesion stress can be typically considered as the interfacial adhesion strength of the interface [Niu, Wang, Wang, and Tian (2009)], implying that the delamination, crack and even fracture phenomena are likely to occur at the interface as the interfacial stress is larger than interfacial adhesion strength.

Table 2 demonstrates the calculated interfacial adhesion strengths for all interfaces on the micro-bump interconnect at the electric field of 0.05 and 0.1 V/Å. It is evident that the interfacial adhesion strengths at the interfaces on the top half of the micro-bump interconnect are larger than those of the bottom half of micro-bump interconnect as the electric field is applied on the micro-bump along the direction of [0 0 1]. The results also indicate the all interfacial adhesion strengths for all interfaces in the micro-bump interconnect reduce with the increasing electric field.

Table 2 further shows that the interface between wetting layer and diffusion barrier layer possesses the strongest interfacial adhesion strength, followed by the interface between diffusion barrier layer and adhesion layer, and the interface between solder bump and wetting layer. Thus, it is deduced that the interfacial failure is prone to occur at the interface between solder bump and wetting layer as the external electric field is imposed on the micro-bump interconnect, suggesting that the interface between solder bump and wetting layer would hold the worst electromigration resistance ability as compared to the other interfaces. In addition, it is noted

that the Sn-3.5Ag/Cu/Ni micro-bump interconnect would hold the largest interfacial adhesion strength between solder bump and wetting layer (i.e., $\sigma^{top}_{\text{Sn-3.5Ag/Cu}}$ and $\sigma^{bottom}_{\text{Sn-3.5Ag/Cu}}$) at the electric field of 0.05 V/Å, which are approximately 17.39 and 12.08 GPa. This reveals that as the micro-bump interconnect is composed of Sn-3.5Ag/Cu/Ni, its interface between solder bump and wetting layer possesses much better electromigration resistance ability as compared to Sn-3.5Ag/Cu/Ni/Cr, Sn-3.5Ag/Cu/TiW and Sn-3.5Ag/Cu/V/Cr micro-bump interconnects.

The calculated results in Table 2 also exhibit the interfacial adhesion strength between wetting layer and diffusion barrier. It is found that as the Ni metal acts as the diffusion barrier layer, it holds the much better interfacial adhesion strength with copper layer as compared to TiW and V metals. Moreover, as the Cr metal is acted as the adhesion layer, the Ni metal, acting as diffusion barrier layer, possesses much larger interfacial adhesion strength than that of V metal. Finally, both calculated interfacial adhesion stress and average bond length, for estimating the electromigration resistance ability, are in good agreement with each other.

4 Conclusions

In summary, by evaluating the average bond length and interfacial adhesion stress of the Sn-3.5Ag/Cu/Ni, Sn-3.5Ag/Cu/TiW, Sn-3.5Ag/Cu/Ni/Cr and Sn-3.5Ag/Cu/V/Cr micro-bump interconnect systems through the DFT calculation, the interfacial adhesion strength between solder bump and UBMs can be extensively explored. Additionally, the electric field is applied on the micro-bump interconnect systems such that the solder bump and UBM with better interfacial adhesion strength and electromigration resistance ability can then be determined.

The results show that as the micro-bump interconnect is composed of Sn-3.5Ag/Cu/Ni, its interface between solder bump and wetting layer possesses much better electromigration resistance ability as compared to Sn-3.5Ag/Cu/Ni/Cr, Sn-3.5Ag/Cu/TiW and Sn-3.5Ag/Cu/V/Cr micro-bump interconnects. Besides, as the diffusion barrier layer is made of Ni metal, it possesses much better interfacial adhesion strength with copper layer as compared to TiW and V metals. Finally, as the adhesion layer is composed of Cr metal, the Ni metal, acting as diffusion barrier layer, has much larger interfacial adhesion strength than that of V metal.

Acknowledgement: The work is partially supported by Ministry of Science and Technology, Taiwan, ROC, under grants MOST 103-2221-E-007-010- and MOST 104-2221-E-007-010-. The authors would also like to thank the National Center for High-Performance Computing (NCHC) for computational resources support.

References

Branden, B. K.; Cristian, V. C. (2013): Bandgap opening in metallic carbon nanotubes due to silicon adatoms. *Computers, Materials & Continua*, vol. 38, no. 1, pp. 1–16.

Brillouin, L. (1930): Les électrons dans les métaux et le classement des ondes de de Broglie correspondantes. *Comptes Rendus Hebdomadaires des Séances de l'Académie des Sciences*, vol. 191, pp. 292–294.

Chen, W. H.; Yu, C. F.; Cheng, H. C.; Tsai, Y. M.; Lu, S. T. (2013): IMC growth reaction and its effects on solder joint thermal cycling reliability of 3D chip stacking packaging. *Microelectronics Reliability*, vol. 53, pp. 30–40.

Chen, W. H.; Yu, C. F.; Chiang K. N.; Cheng, H. C. (2015): First-principles density functional calculations of physical properties of orthorhombic Au_2Al crystal. *Intermetallics*, vol. 62, pp. 60–68.

Cheng, H. C.; Tsai, Y. H.; Chen, K. N.; Fang, **J.** (2010): Thermal placement optimization of multichip modules using a sequential metamodeling-based optimization approach. *Applied Thermal Engineering*, vol. 30, pp. 2632–2642.

Cheng, H. C.; Hsieh, K. Y.; Chen, **K. M.** (2011)**:** Thermal-mechanical optimization of a novel nanocomposite-film typed flip chip technology. *Microelectronics Reliability*, vol. 51, pp. 826–836.

Cheng, H. C.; Cheng, H. K.; Lu, S. T.; Juang, J. Y.; Chen, W. H. (2014): Drop impact reliability analysis of 3-D chip-on-chip packaging: Numerical modeling and experimental validation. *IEEE Transactions on Device and Materials Reliability*, vol. 14, pp. 499–511.

Cheng, H. C.; Yu, C. F.; Chen, W. H. (2014a): On the first-principles density functional theory calculation of electromigration resistance ability for Sn-based intermetallic compounds. *Computer Modelling Engineering & Sciences*, vol. 100, pp. 119–131.

Cheng, H. C.; Yu, C. F.; Chen, W. H. (2014b): Physical, mechanical, thermodynamic and electronic characterization of $Cu_{11}In_9$ crystal using first-principles density functional theory calculation. *Computational Materials Science*, vol. 81, pp. 146–157.

Fan, H. B.; Yuen, M. F. (2010): A multi-scale approach for investigation of interfacial delamination in electronic packages. *Microelectronics Reliability*, vol. 50, pp. 893–899.

Gerstle, W.; Silling, S.; Read, D.; Tewary, V.; Lehoucq, R. (2008): Peridynamic simulation of electromigration. *Computer Modeling in Engineering & Sciences*, vol. 8, pp. 75–92.

Head, J. D. (1985): A Broyden-Fletcher-Goldfarb-Shanno optimization procedure for molecular geometries. *Chemical Physics Letters*, vol. 122, pp. 264–270.

Hohenberg, P.; Kohn, W. (1964): Inhomogeneous electron gas. *Physical Review*, vol. 136, pp. 864–871.

Hu, H. C.; Cheng, H. C.; Huang, T. C.; Chen, W. H.; Wu, S. T.; Lo, W. C. (2015): On the thermal performance analysis of three-dimensional chip stacking electronic packaging with through silicon vias. *International Conference on Electronic Packaging and iMAPS All Asia Conference*, pp. 532–537.

Iwasaki, T.; Miura, H. (2003): Molecular-dynamics analysis of grain-boundary grooving in interconnect films with underlayers. *Computer Modeling in Engineering & Sciences*, vol. 4, pp. 551–557.

Monkhorst, H. J.; Pack, J. D. (1976): Special points for Brillouin-zone integrations. *Physical Review B*, vol. 13, pp. 5188–5192.

Nielsen, O. H.; Martin, R. M. (1987): Quantum-mechanical theory of stress and force. *Physical Review B*, vol. 32, pp. 3780–3791.

Niu, J. G.; Wang, B. J.; Wang, C. B.; Tian, X. (2009): First-Principles calculation of electronic structure, bonding characteristic and bonding strength of TiN (111)/BN/TiN (111) interface. *Acta Metallurgical Sinca*, vol. 45, pp. 1185–1189.

Patterson, D. S.; Elenius, P.; Leal, J. A. (1997): Wafer bumping technologies-A comparative analysis of solder deposition processes and assembly considerations. *Advances in Electronic Packaging*, vol. 1, pp. 337–351.

Perdew, J. P.; Burke, K.; Ernzerhof, M. (1996): Generalized gradient approximation made simple. *Physical Review Letter*s, vol. 77, pp. 3865–3868.

Vanderbilt, D. (1990): Soft self-consistent pseudopotentials in a generalized eigenvalue formalism. *Physical Review B*, vol. 41, pp. 7892–7895.

Wu, X.; Paik, W.; Bhandarkar, S. N. (1995): To cut or not to cut: a thermomechanical stress analysis of Polyimide thin-film on ceramic structure. *IEEE Transactions on Component, Packaging, and Manufacturing Technology*, vol. 18, pp. 150–153.

Yang, P. F.; Lai, Y. S.; Jian, S. R.; Chen, J. (2007): Mechanical properties of Cu_6Sn_5, Cu_3Sn, and Ni_3Sn_4 intermetallic compounds measured by nanoindentation. *International Conference on Electronics Packaging Technology*, pp. 1–5.

Yu, C. F.; Cheng, H. C.; Chen, W. H. (2015): Structural, mechanical and thermodynamic properties of $AuIn_2$ crystal under pressure: A first-principles density functional theory calculation. *Journal of Alloys and Compounds*, vol. 619, pp. 576–584.

Zhu, L.; Zhou, J.; Fan, X. (2014): Rupture and instability of soft films due to moisture vaporization in microelectronic devices. *Computers, Materials & Continua*, vol. 39, no. 2, pp. 113–134.